Porous Materials **Hot Paper**

The First Sulfate-Pillared Hybrid Ultramicroporous Material, SOFOUR-1-Zn, and Its Acetylene Capture Properties

Debobroto Sensharma, Daniel J. O'Hearn, Amin Koochaki, Andrey A. Bezrukov, Naveen Kumar, Benjamin H. Wilson, Matthias Vandichel, and Michael J. Zaworotko*

Abstract: *Hybrid ultramicroporous materials, HUMs, are comprised of metal cations linked by combinations of inorganic and organic ligands. Their modular nature makes them amenable to crystal engineering studies, which have thus far afforded four HUM platforms (as classified by the inorganic linkers). HUMs are of practical interest because of their benchmark gas separation performance for several industrial gas mixtures. We report herein design and gram-scale synthesis of the prototypal sulfate-linked HUM, the **fsc** topology coordination network ($[Zn(tepb)(SO_4)]_n$), **SOFOUR-1-Zn**, tepb = (tetra(4-pyridyl)benzene). Alignment of the sulfate anions enables strong binding to C_2H_2 via O···HC interactions but weak CO_2 binding, affording a new benchmark for the difference between C_2H_2 and CO_2 heats of sorption at low loading ($\Delta Q_{st} = 24 \, kJ \, mol^{-1}$). Dynamic column breakthrough studies afforded fuel-grade C_2H_2 from trace (1:99) or 1:1 C_2H_2/CO_2 mixtures, outperforming its SiF_6^{2-} analogue, **SIFSIX-22-Zn**.*

Introduction

The amenability of metal–organic materials (MOMs) to design from first principles has afforded families of porous coordination networks (PCNs) with excellent properties for physisorptive separations.[1] In this context, hybrid ultramicroporous materials (HUMs) have emerged as an especially attractive class of PCNs. HUMs are typically comprised of an organic linker, an anionic inorganic linker, and a metal node. Their combination of ultramicropores (<7 Å diameter) and pore chemistry (strong electrostatics from the inorganic pillars that line pore walls) can afford highly selective binding sites for gaseous adsorbates.[2] The inherent

[*] Dr. D. Sensharma, D. J. O'Hearn, A. Koochaki, Dr. A. A. Bezrukov, Dr. N. Kumar, Dr. B. H. Wilson, Dr. M. Vandichel, Prof. M. J. Zaworotko
Department of Chemical Sciences, Bernal Institute
University of Limerick, Limerick V94 T9PX (Republic of Ireland)
E-mail: xtal@ul.ie

A. Koochaki, Prof. M. J. Zaworotko
Advanced Materials and Bioengineering Research (AMBER) Centre
Dublin D02 R590 (Republic of Ireland)

modularity of HUMs is advantageous since it enables first generation HUMs to be systematically developed into sorbent families (platforms) with optimised pore sizes and chemistries. Such a crystal engineering approach offers insight into structure-function relationships and means that second generation HUMs can offer a degree of control over binding sites and energies that is not readily available in traditional classes of sorbent such as zeolites and porous carbons.[3]

Most HUMs follow a simple structural blueprint in which divalent metal cations are 4-connected at their equatorial positions by four neutral ditopic organic linkers, thereby forming a cationic square lattice (**sql**) topology coordination network. The axial positions of the metal centres are further linked by inorganic dianion "pillars" to yield a neutral primitive cubic, **pcu**, topology network. For example, in the archetypal HUM, **SIFSIX-1-Zn**, the metal cation is Zn^{2+}, the organic linker is 4,4′-bipyridine, and the inorganic pillar is SiF_6^{2-}.[4] These building blocks can be substituted to produce new HUMs in a highly modular fashion: Zn^{2+} can be substituted by other M^{2+} cations (e.g. Cu^{2+}, Ni^{2+}, Cd^{2+}); 4,4′-bipyridine can be replaced by longer (e.g. *N,N′*-di(4-pyridyl)-1,4,5,8-naphthalene diimide, 15.4 Å) or shorter (e.g. pyrazine, 2.8 Å) organic ligands; distinct platforms are then defined by the type of inorganic pillar used, e.g. **MFSIX** (e.g. TiF_6^{2-}, SnF_6^{2-}), **FOXY** (e.g. $NbOF_5^{2-}$), **M′FFIVE** (e.g. AlF_5^{2-}), and **DICRO** ($Cr_2O_7^{2-}$), can replace SiF_6^{2-}.[5] Although most HUMs are constructed in this manner, other topologies can exist: the **mmo** platform;[6] **Tripp-Cu-MFSIX** ($[Cu_6(Tripp)_8](MF_6)_3(MF_6)_3]_n$), **Tripp** = 2,4,6-tris(4-pyridyl)pyridine) is based upon a tritopic ligand;[7] the **fsc** networks **CPM-131** and **fsc-2-SIFSIX** are sustained by tetratopic ligands.[8] The recently reported **fsc** network **ZJU-280** exploited the tetratopic ligand tetra(4-pyridyl)benzene (**tepb**) and was found to exhibit promising C_2H_2/C_2H_4 separation capabilities.[9]

HUMs are particularly amenable to crystal engineering, even compared to most MOFs,[3] enabling systematic fine-tuning of pore size and pore chemistry and optimisation of key properties such as selectivity and working capacity. Indeed, the current top-performing sorbents for several industrially important gas mixtures are HUMs: **SIFSIX-18-Ni-β**, **NbOFFIVE-1-Ni** and **TIFSIX-3-Ni** for CO_2/N_2;[10] **NbOFFIVE-1-Ni** and **TIFSIX-3-Ni** for CO_2/CH_4;[11] **SIFSIX-14-Cu-i** for C_2H_2/C_2H_4[12] **DICRO-4-Ni-i**, **TIFSIX-2-Cu-i**, **UTSA-300**, **SIFSIX-21-Ni** and **BSF-3** for C_2H_2/CO_2;[13] and **CROFOUR-1-Ni** for Xe/Kr.[14] The selection of the inorganic pillar is crucial since it is more than a structural

component; pillars form the binding site that enables selective sorption. The use of such anionic pillars to form binding sites sets HUMs apart from other classes of porous coordination networks such as MOFs, which tend to rely upon coordinatively unsaturated metal centres (UMCs) to provide selective adsorbate binding. Importantly, the non-covalent sorbate-sorbent interactions in HUMs tend to be weaker than UMCs and can lie in a thermodynamic "sweet spot" that allows benchmark selectivity to be combined with low energy desorption. Nevertheless, despite their ability to generate highly selective binding, fluorinated anion pillars can present challenges in terms of synthesis methodology (e.g. use of HF in production), cost and corrosivity (e.g. hydrolytic or thermal decomposition).[15] Other pillars, such as $Cr_2O_7^{2-}$, CrO_4^{2-}, and MoO_4^{2-} comprise toxic metals, and the boron oxyanions used in **BSF-3** and the recently reported **ZNU-1** are relatively intricate and costly.[6a, 13e, 16]

There is therefore a need to generate HUMs using earth-friendly inorganic anions while retaining sorption performance. The sulfate anion (**SOFOUR**) is cheap, divalent, and metal/fluoride free, making it an ideal candidate for such studies. Herein, we report the first example of a **SOFOUR** HUM along with its gas sorption properties and separation performance for C_2H_2, acetylene, over CO_2.

We chose to study C_2H_2/CO_2 as it is among the most challenging of gas separations. Since its discovery in Ireland in the 1830s, acetylene has become a very widely produced chemical commodity with industrial utility as a chemical feedstock and fuel.[17] Fuel applications require $>98\%$ pure C_2H_2 and use as a feedstock requires even higher purities. However, the predominant processes by which acetylene is produced utilize partial oxidation of alkanes, in which CO_2 is produced as a by-product and a persistent contaminant.[17b,c,18] In such processes, the absence of oxygen leads to soot formation, and thus the production of CO and CO_2 necessarily accompanies C_2H_2 production. Although most C_2H_2/CO_2 separation studies focus on 1:1 and 2:1 C_2H_2/CO_2 mixtures, the yields of the production routes are variable and depend on several factors including feed-stock type and purity, oxygen content, temperature, and process considerations.[17b,c] For instance, high temperature plasma pyrolysis techniques using CH_4 feeds may have C_2H_2 yields as high as 80–90%, coal-based processes can show yields between 20 and 80%, the BASF controlled partial oxidation process has yields of 10–33%, whereas other methods may have even lower yields, e.g. propane cracking yields only 2% C_2H_2.[17c,18] Typically, higher yields are achieved under more demanding conditions and higher temperatures. Therefore, studies considering equimolar mixtures serve as representative examples of C_2H_2/CO_2 separations, but may not address the greater challenge of viably capturing and purifying acetylene from lower-yield outputs.

Although the by-product profiles in each case are different, CO_2 is an important and persistent contaminant, especially in production routes involving partial combustion. The separation of CO_2 from C_2H_2 is challenging due to similar physicochemical properties such as boiling point

(194.7 K for CO_2, 188.4 K for C_2H_2) and quadrupole moment (4.3×10^{-26} esu cm^2 for CO_2, 3.0×10^{-26} esu cm^2 for C_2H_2). In addition, they have similar molecular dimensions ($3.32 \times 3.34 \times 5.7$ Å^3 for CO_2, $3.18 \times 3.33 \times 5.36$ Å^3 for C_2H_2) and kinetic diameters (3.3 Å for both CO_2 and C_2H_2).[19] Further, C_2H_2 is explosive, so it is unsafe to liquefy in cryogenic purification processes such as those used for C_2H_4 and other hydrocarbons. Consequently, energy-intensive gas–liquid absorption methods are used for the purification of C_2H_2, e.g. with solvents such as *N*-methyl pyrrolidone, *N,N*-dimethyl formamide, methanol, and acetone or alkaline scrubbing agents for chemical removal of CO_2. There is a large environmental cost and owing to the scale of C_2H_2 production (projected market value of 6.9 billion USD in 2025), even minor improvements to the economics and ecological footprints of these processes could result in major savings.[20] In addition, the extremely low flammability limit of acetylene in mixtures (2.5%) discourages the recirculation of partially separated mixtures and can necessitate the trace removal of acetylene from gas streams for safety reasons.[21] In order to address the problem of separations in acetylene-poor mixtures and feeds below the flammability limit, a number of recent studies have examined the viability of trace C_2H_2/CO_2 separations (1:99) by dynamic column breakthrough (DCB) studies.[2,22] However, the physisorptive recovery of acetylene of commercial grade from low concentration mixtures of C_2H_2 with CO_2 has not previously been demonstrated.

The thermodynamic "sweet spot" for C_2H_2/CO_2 selective HUMs arises from arrangements of fluorinated inorganic anion pillars. Optimised geometries can enable molecular recognition of C_2H_2 via H-bonding as seen for HUMs like **SIFSIX-21-Ni**, **TIFSIX-2-Cu-i** and **ZNU-1**.[13b,d,e] However, when C_2H_2 is preferentially adsorbed, the production of pure C_2H_2 requires desorption of C_2H_2 from the adsorbent and is operationally challenging. Sorbents with "inverse" selectivity, in which CO_2 is adsorbed preferentially over C_2H_2, have been studied as they can produce a pure C_2H_2 effluent stream (eg. **SIFSIX-3-Ni**, **Tm(OH-bdc)**, **Cd-NP**, and **CD-MOF-2**).[13b,23] Unfortunately, trace C_2H_2 streams present a limitation due to the rapid saturation of the adsorbent bed with CO_2. The optimum adsorbent for capture of C_2H_2 from dilute feeds would therefore exhibit high C_2H_2 uptake at low partial pressures, preferential C_2H_2 binding, and facile regeneration allowing the recovery of high-purity C_2H_2 during desorption. In this contribution, we address both the challenge of efficient trace C_2H_2/CO_2 separation and the need for a cheap, green alternative inorganic pillar for HUMs.

Results and Discussion

Among the possible divalent anion pillars for possible utility as HUM pillars, sulfate anions stand out as they are exceptionally cheap, non-toxic, and amenable for use at large scale. Further, the related tetrahedral dianions CrO_4^{2-} and MoO_4^{2-} form HUMs that exhibit 6-connected $4^8.6^7$ **mmo** topology.[6] In order to generate a HUM based on pillared

sqls with channels comparable to those in **pcu** topology HUMs, we selected the tetratopic ligand **tepb** (tetra(4-pyridyl)benzene) and Zn^{2+} nodes. Single crystals of the target HUM, **[Zn(tepb)(SO$_4$)]$_n$**, **SOFOUR-1-Zn**, were obtained by layering and studied by single crystal X-ray diffraction. In addition, the SiF_6^{2-} pillared analogue, **SIFSIX-22-Zn**, was prepared using the same methodology to serve as reference point for performance evaluation.

SOFOUR-1-Zn crystallised in the orthorhombic space group *Cmm2*. Its structure is a (4,6)-connected **fsc** topology network (Figure 1a, b) in which each octahedral Zn^{2+} moiety serves as a 6-c node and each **tepb** ligand serves as a 4-c node. Each Zn^{2+} moiety is coordinated by two ditopic bridging sulfate anions at the axial positions whereas the equatorial positions are occupied by four tetratopic **tepb** ligands. Notably, the SO_4^{2-} anions serve as pillars between Zn-**tepb** 2-dimensional **sql**s to afford an **fsc** topology net (Figure S1). The sulfate anions are disordered over two positions, suggesting they can rotate and modify the pore environment (see Supporting Information for refinement details).[24] Figure 1e reveals the outcome of a Cambridge Structural Database (CSD version 5.41 (2019+3 updates)) survey that plots pillaring angle (pillar = SiF_6^{2-} or SO_4^{2-}) vs. M⋯ bridging distance of the pillar.[25] The pillaring angle for **SOFOUR-1-Zn** is close to linear, at 173.5(3)°, higher than 98% of the pillaring angles for SO_4^{2-} (Figure 1e). As expected, for SO_4^{2-} there is a positive correlation between pillaring angle and M⋯M distance; **SOFOUR-1-Zn** fits this trend, having a relatively large M⋯M distance of 6.5163(2) Å, higher than 90% of previously reported Zn-based structures. Further details of the CSD survey and analysis are presented in the Supporting Information.

SIFSIX-22-Zn, **[Zn(tepb)SiF$_6$]$_n$**, crystallised in the orthorhombic space group *Cmma* and is isostructural to the recently reported Cu-based **ZJU-280**.[9] The pyridyl rings of the **tepb** ligands in both **SOFOUR-1-Zn** and **SIFSIX-22-Zn**

(Figure 1a, b and c, d, respectively) are arranged in a propeller conformation around the Zn^{2+} metal centre. The dihedral angle between opposite rings for **SOFOUR-1-Zn** is 70.72(17)° and 59.10(14)° for adjacent rings whereas for **SIFSIX-22-Zn**, the angles are 59.08(9)°, and 64.65(8)°, respectively. Similarly, the pyridyl rings are also arranged in a propeller conformation around the phenyl ring of the **tepb** ligand with dihedral angles with the phenyl ring of 49.4(2)° and 51.8(2)° for the two crystallographically distinct pyridyl rings in **SOFOUR-1-Zn**, and 56.02(8)° for the one crystallographically distinct pyridyl ring in **SIFSIX-22-Zn**. Despite the differences in dihedral angles, the ligands from both **SOFOUR-1-Zn** and **SIFSIX-22-Zn** overlay closely with overlap of the atomic ellipsoids drawn at the 50% probability level for every atom (Figure S2). The interlayer distance is 7.5678(9) Å is **SIFSIX-22-Zn** vs. 6.5163(2) Å in **SOFOUR-1-Zn**.

A CSD survey revealed that 1479 SO_4^{2-} bridged coordination polymers have been reported.[25] Of these, only 136 were found to have four nitrogen atoms coordinated to a metal centre (Figure S5, S6, Table S2). Permanent porosity was demonstrated experimentally through gas sorption experiments in just five: **[Cd(Tppa)(SO$_4$)(H$_2$O)]**, **[Cd$_2$(tpim)$_4$(SO$_4$)(H$_2$O)$_2$]·(SO$_4$)]**, **[Co$_2$(bpy)$_3$(SO$_4$)$_2$(H$_2$O)$_2$](bpy)]**, **[Cd$_2$L$_4$(SO$_4$)(H$_2$O)]·(SO$_4$)]** and **[Zn$_2$L$_4$(SO$_4$)(H$_2$O)$_2$]·(MeOSO$_3$)]** (Tppa = tris(4-(pyridyl)-phenyl) amine, **tpim**, **L** = 2,4,5-tri(4-pyridyl)imidazole, **bpy** = 4,4'-bipyridine), each of which is distinct in terms of structure.[26] Additionally, the 3,5-connected net of formula **[Cu(tepb)(SO$_4$)]** has been reported without sorption data and is also distinct from the 4,6-connected **fsc** net reported herein.[27] To our knowledge, **SOFOUR-1-Zn** is not only prototypal for a new HUM platform, it is the first SO_4^{2-}-based porous coordination network of any type to be studied for gas separations.

Gram-scale quantities of **SOFOUR-1-Zn** were synthesised by stirring zinc(II) sulfate and **tepb** in MeOH at room temperature. The resulting microcrystalline white powder was
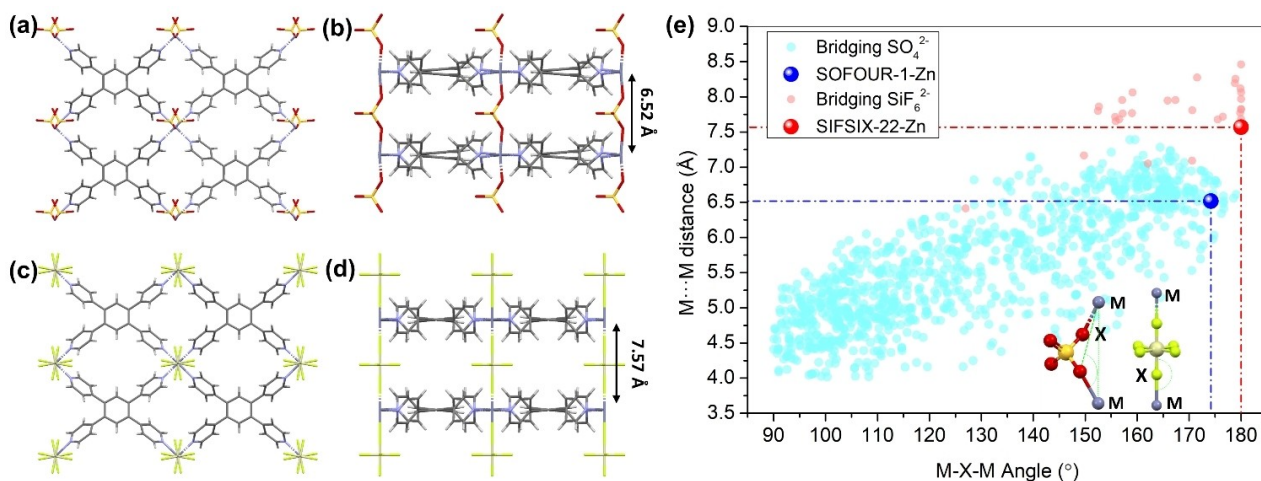

Figure 1. a) Crystal structure of **SOFOUR-1-Zn** viewed along the crystallographic *a*-axis; b) viewed along the crystallographic *b*-axis; c) viewed along the crystallographic *a*-axis; d) **SIFSIX-22-Zn** viewed along the crystallographic *b*-axis; e) a scatter plot of the results for a CSD search of M⋯M distances for SO_4^{2-} and SiF_6^{2-} pillars versus the angle between one of the coordinating atoms (X = O, F) and the bridged metals (M = Mn, Fe, Co, Ni, Cu, Zn, Cd).

characterised by powder X-ray diffraction and thermogravimetric analysis, which indicated phase purity and thermal stability up to ca. 300 °C (Figure S3, S4). An initial solvent loss of 10.5 wt.% was observed below 100 °C, corresponding to loss of MeOH from the as-synthesized structure. CO_2 sorption at 195 K enabled determination of BET surface areas, 612.1 m²g⁻¹ for **SOFOUR-1-Zn** and 641.0 m²g⁻¹ for **SIFSIX-22-Zn** (Figure 2a). Pore-size distributions calculated from these isotherms by the Horvath–Kawazoe method indicated maximum pore widths for **SIFSIX-22-Zn** and **SOFOUR-1-Zn** at 4.1 Å and 4.0 Å respectively, validating them as ultramicroporous (Figure 2b).

Isotherms measured on **SIFSIX-22-Zn** at 298 K showed type I characteristics with uptakes for CO_2 of 95 cm³g⁻¹ and 127 cm³g⁻¹ for C_2H_2. Whereas **SOFOUR-1-Zn** exhibited a lower 1 bar uptake for C_2H_2 (69 cm³g⁻¹) than CO_2 (81 cm³g⁻¹), its high C_2H_2 uptake at lower pressures is indicative of strong C_2H_2 binding sites. Specifically, at 298 K and 0.01 bar, **SOFOUR-1-Zn** had uptakes of 1.65 mmol g⁻¹ of C_2H_2 and 0.20 mmol g⁻¹ of CO_2 (Figure 2c). This low pressure C_2H_2 uptake is comparable to top-performing acetylene sorbents such as **MUF-17** (1.40 mmol g⁻¹), **NKMOF-1-Ni** (1.74 mmol g⁻¹), **TIFSIX-2-Cu-i** (1.78 mmol g⁻¹), and **UTSA-200a** (1.83 mmol g⁻¹).[12,13b,22a,28] Experimentally determined isosteric heats of adsorption (Q_{st}) for **SOFOUR-1-Zn** (33 kJ mol⁻¹ for CO_2, 57 kJ mol⁻¹ for C_2H_2 at low loading, Figure 2d), S7–S10 are consistent with experimental uptakes at low pressures. The difference in Q_{st} values between C_2H_2 and CO_2 (ΔQ_{st}), 24 kJ mol⁻¹, is to our knowledge the highest yet

reported for a physisorbent (**NKMOF-1-Ni** = 19.4 kJ mol⁻¹, **CPL-1-NH$_2$** = 17.6 kJ mol⁻¹, **BSF-3** = 17.2 kJ mol⁻¹, **sql-16-Cu-NO$_3$-α'** = 13.0 kJ mol⁻¹).[13e,28,29] Low-loading Q_{st} values for **SIFSIX-22-Zn** were determined to be 36.5 kJ mol⁻¹ for C_2H_2 and 25 kJ mol⁻¹ for CO_2, a ΔQ_{st} of 11.5 kJ mol⁻¹.

Ideal Adsorbed Solution Theory (IAST) calculations using 298 K isotherms indicated that **SOFOUR-1-Zn** and **SIFSIX-22-Zn** display similar C_2H_2/CO_2 selectivities (S_{AC}) of ca. 6.60 and 6.49 respectively for equimolar mixtures at 1 bar (Figure 2e). The calculated selectivity is nearly constant for **SIFSIX-22-Zn** for compositions of 10 % (7.08), 5 % (7.23), and 1 % C_2H_2 in CO_2 (7.36). Conversely, selectivity values increase for **SOFOUR-1-Zn** (9.55 for 10 %, 10.85 for 5 % and 13.00 for 1 %), indicating potential for trace removal. The differences between **SOFOUR-1-Zn** and **SIFSIX-22-Zn** in terms of their sorption characteristics can be attributed directly to the use of the SO_4^{2-} pillar and its effects on interlayer distance and pore electrostatics. Temperature swing cycling experiments conducted gravimetrically under C_2H_2 and CO_2 flow conditions revealed that the adsorption performance of **SOFOUR-1-Zn** and **SIFSIX-22-Zn** was retained in successive cycles. Further, the sorbents were regenerated through a 303 K to 363 K temperature swing (Figure S11). Initial adsorption rates indicated that both **SOFOUR-1-Zn** and **SIFSIX-22-Zn** exhibited faster uptake kinetics for C_2H_2 than for CO_2, favouring **SOFOUR-1-Zn** over **SIFSIX-22-Zn** (Figure S12). Specifically, in the first 2.5 minutes of adsorption, **SOFOUR-1-Zn** adsorbed C_2H_2 equivalent to 20.0 % of its 1 bar saturation uptake, but only
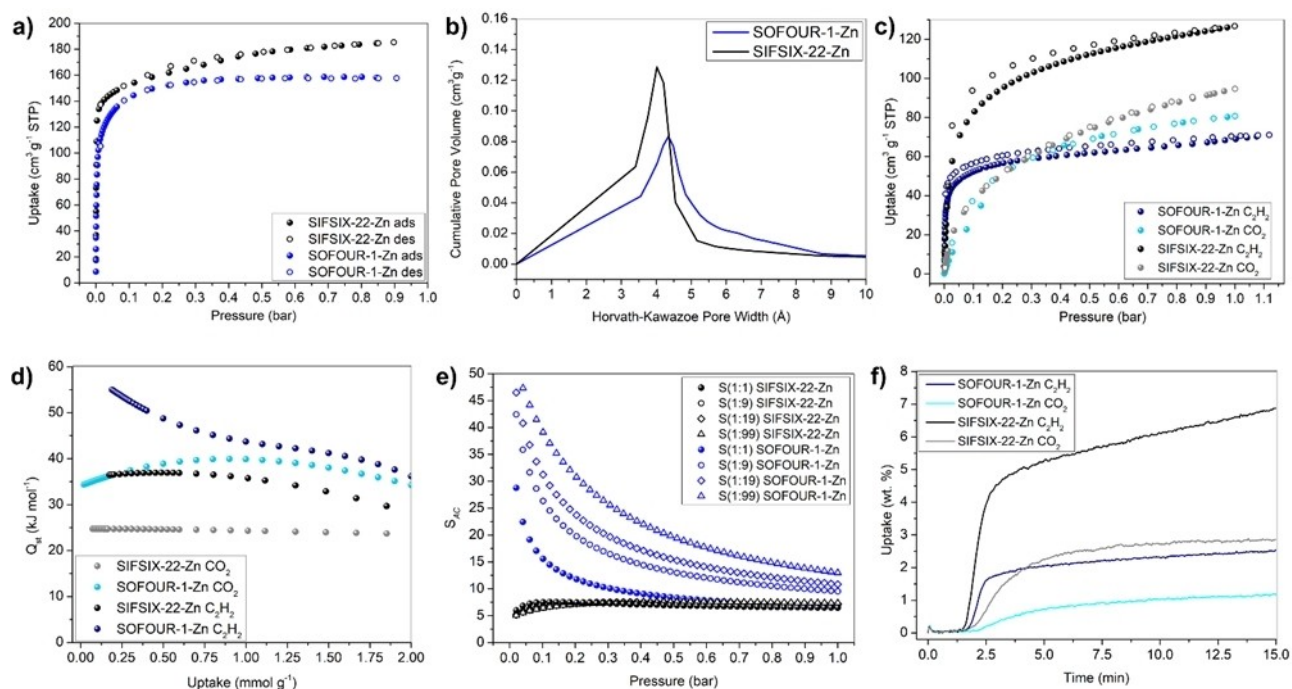

Figure 2. a) The 195 K CO_2 sorption isotherms of **SOFOUR-1-Zn** and **SIFSIX-22-Zn**; b) Horvath–Kawazoe pore-size distributions of **SOFOUR-1-Zn** and **SIFSIX-22-Zn** calculated from the 195 K CO_2 sorption isotherms; c) 298 K C_2H_2 and CO_2 isotherms of **SOFOUR-1-Zn** and **SIFSIX-22-Zn**; d) coverage-dependent isosteric heats of C_2H_2 and CO_2 for **SOFOUR-1-Zn** and **SIFSIX-22-Zn**; e) C_2H_2/CO_2 IAST selectivities of **SOFOUR-1-Zn** and **SIFSIX-22-Zn** at 298 K for various compositions vs. pressure; f) gravimetric kinetics of C_2H_2 and CO_2 sorption on **SOFOUR-1-Zn** and **SIFSIX-22-Zn** plotted as uptake vs. time.

1.2 % of its CO_2 uptake. Kinetics of adsorption in **SIFSIX-22-Zn** are faster but less discriminatory, with 2.5 minute loading equal to 31.5 % and 4.1 % of C_2H_2 and CO_2 saturation uptakes, respectively (Figure 2f).

These properties suggest **SOFOUR-1-Zn** as a candidate for trace C_2H_2/CO_2 separations. Indeed, comparison with leading C_2H_2/CO_2-selective sorbents ($S_{AC} > 5$) that do not use chemisorptive or UMC binding sites revealed that **SOFOUR-1-Zn** is one of just four MOMs with a C_2H_2 Q_{st} value in the "sweet spot" between 45 and 60 kJ mol^{-1} that allows both strong binding and energy-efficient regeneration.[2] Among these, **SOFOUR-1-Zn** is the only adsorbent with a ΔQ_{st} greater than 20 (Figure 3). Therefore,

despite its modest S_{AC} value, when this is coupled with a kinetic preference for C_2H_2 over CO_2, **SOFOUR-1-Zn** is highly suited to C_2H_2/CO_2 separation at low partial pressures of C_2H_2.

In order to experimentally validate the separation performance of **SOFOUR-1-Zn** under mixed-gas conditions, we conducted dynamic column breakthrough (DCB) experiments using a fixed bed and gas mixture compositions between 50 % C_2H_2 and 1 % C_2H_2 at ambient conditions (Figure 4). Identical experimental conditions were used for **SIFSIX-22-Zn** as a reference point. We indeed determined that **SOFOUR-1-Zn** separated an equimolar C_2H_2/CO_2 mixture at a combined flow rate of 1 sccm and ambient

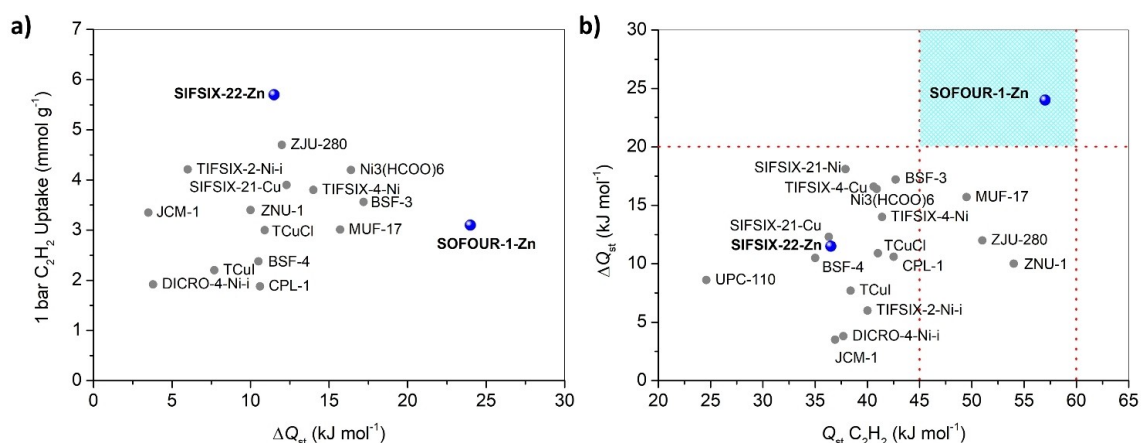**Figure 3.** a) 1 bar C_2H_2 uptake versus low loading ΔQ_{st} (C_2H_2–CO_2) for leading C_2H_2/CO_2 selective physisorbents; b) low loading ΔQ_{st} (C_2H_2–CO_2) vs. low loading C_2H_2 Q_{st} for leading C_2H_2/CO_2 selective physisorbents; **SOFOUR-1-Zn** is the only sorbent with $\Delta Q_{st} > 20$ and C_2H_2 Q_{st} from 45–60 kJ mol^{-1}.
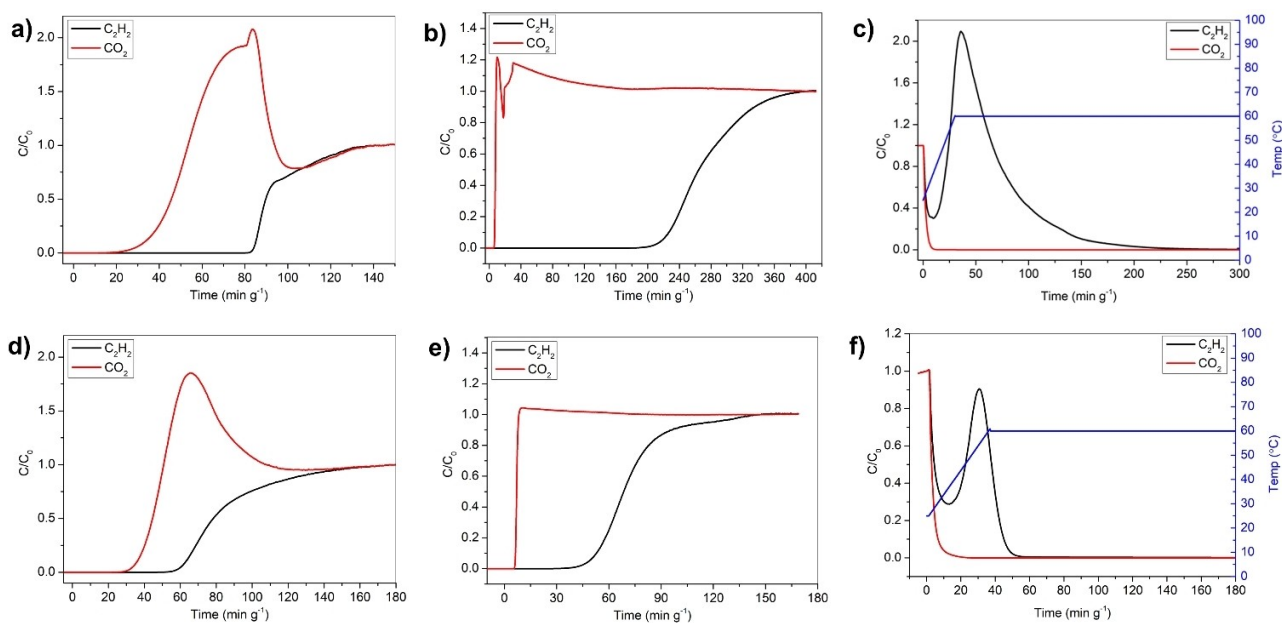

Figure 4. C_2H_2/CO_2 DCB curves for **SOFOUR-1-Zn** with inlet flows of a) 1:1 C_2H_2:CO_2, 1 sccm; b) 1:99 C_2H_2:CO_2, 7 sccm; c) C_2H_2/CO_2 TPD curves for **SOFOUR-1-Zn** after saturation with an inlet flow of c) 1:99 C_2H_2:CO_2, 7 sccm; C_2H_2/CO_2 DCB curves for **SIFSIX-22-Zn** with inlet flows of d) 1:1 C_2H_2:CO_2, 1 sccm; e) 1:99 C_2H_2:CO_2, 7 sccm; f) C_2H_2/CO_2 TPD curves for **SIFSIX-22-Zn** after saturation with an inlet flow of 1:99 C_2H_2:CO_2, 7 sccm.

conditions with breakthrough times of ca. 22 min g^{-1} for CO_2 and ca. 83 min g^{-1} for C_2H_2. The separation factor (α_{AC}) was calculated to be 17.5, higher than some leading C_2H_2 selective adsorbents, such as **ZJU-74a** (4.3), **HOF-3a** (2.0), and **NKMOF-1-Ni** (2.6), but lower than benchmark sorbents such as the **TCuX** series (33.4–143.1), **IPM-101** (22.5) and **sql-16-Cu-NO₃-α'** (78).[22b, 28–30] Effluent CO_2 purity was > 99.996 % until the elution of C_2H_2. This is equivalent to CO_2 at N4.5 CP Grade specification. Under the same conditions, **SIFSIX-22-Zn** exhibited α_{AC} of 3.8 and effluent CO_2 purity of > 99.99 %, still a strong performance but not as efficient as **SOFOUR-1-Zn**.

DCB experiments were then conducted using a 1:99 C_2H_2/CO_2 inlet stream. **SOFOUR-1-Zn** exhibited a remarkable breakthrough time of ca. 270 min g^{-1} for C_2H_2 at a total inlet flow rate of 7 sccm. CO_2 broke through the column within 3 min g^{-1}, resulting in calculated uptakes of 21.9 cm^3 g^{-1} of C_2H_2 and 17.4 cm^3 g^{-1} of CO_2, and α_{AC} of 124.6. No other 1:99 α_{AC} DCB experiments have been reported in the literature. The purity of the effluent CO_2 remained > 99.996 % under these conditions. **SIFSIX-22-Zn** exhibited uptakes of 5.6 cm^3 g^{-1} of C_2H_2 and 20.3 cm^3 g^{-1} of CO_2 under the same conditions for α_{AC} of 27.3. At intermediate inlet gas compositions of 5 % and 10 % C_2H_2, α_{AC} values of 42.5 and 52.6 were measured, respectively, for **SOFOUR-1-Zn**, while the values for **SIFSIX-22-Zn** were 11.9 and 15.5, respectively (Figure S13, S14).

Temperature-programmed desorption (TPD) experiments were conducted after saturation in DCB experiments using a He gas stream at 20 sccm and a temperature gradient up to 333 K in order to evaluate the feasibility of recovering purified C_2H_2 by desorption. **SOFOUR-1-Zn** and **SIFSIX-22-Zn** both exhibited rapid desorption of CO_2, followed by peaks associated with desorption of C_2H_2 as the temperature was elevated under both 1:1 and 1:99 conditions (Figure S15, S16). In the 1:1 experiments, much of the C_2H_2 was desorbed with CO_2 at the onset of He flow and C_2H_2 desorption also occurred at elevated temperature. Elution of high purity C_2H_2, > 99.5 %, which exceeds instrument grade specifications of purity (> 99.0 %), occurred from 15 to 41 min g^{-1} for **SOFOUR-1-Zn** and from 17 to 30 min g^{-1} for **SIFSIX-22-Zn**. These values correspond to productivities of 2.07 L kg^{-1} and 1.95 L kg^{-1}. Such productivity equals the desorptive C_2H_2 recovery performance of **ZNU-1** and the peak C_2H_2 purity is comparable to the benchmark set by **TIFSIX-2-Cu-i** (99.9 %).[13b,16] C_2H_2 of purity > 98 % was recovered between 15 and 70 min g^{-1} with a productivity of 3.1 L kg^{-1} using **SOFOUR-1-Zn**, and between 17 and 46 min g^{-1} with a productivity of 3.3 L kg^{-1} using **SIFSIX-22-Zn**. We note that even after adsorptive saturation using a 1:99 mixture, C_2H_2 of purity > 98 % (fuel grade) was obtained by desorption from **SOFOUR-1-Zn** for the period between 33 and 40 min g^{-1} and > 95 % between 33 and 84 min g^{-1}, corresponding to productivities of 1.01 L kg^{-1} and 4.66 L kg^{-1} of > 98 % pure and > 95 % pure C_2H_2, respectively. To our knowledge, this is the first demonstration of physisorptive recovery of fuel grade C_2H_2 from a dilute (1:99) C_2H_2/CO_2 mixture. In contrast, the peak C_2H_2 purity achieved during desorption from **SIFSIX-22-Zn** was

96.7 % (at 30.9 min g^{-1}). We attribute this exceptional performance to the favorable C_2H_2 and CO_2 Q_{st} values and high C_2H_2 uptake at low partial pressure, both of which are enabled by highly selective C_2H_2 binding sites.

We conducted computational studies to gain insight into $SO_4^{2-} \cdots C_2H_2$ interactions. The binding sites in **SOFOUR-1-Zn** derived by density functional theory (DFT) calculations for both gases revealed that the interlayer "mezzanine" region which corresponds to the maximum pore diameter plays a key role (Figure 5, S23, S25, S26). C_2H_2 has two hydrogen bonds with SO_4^{2-} pillars (H···O = 2.56 Å and 2.83 Å) while CO_2 has no close C···O contacts. (C···O = 6.12 Å and 6.76 Å). The low loading adsorption enthalpies at 298 K from DFT calculations for C_2H_2 and CO_2 of −53, and −34 kJ mol^{-1}, respectively, are consistent with the Q_{st} values obtained experimentally. In **SIFSIX-22-Zn**, C_2H_2 has two hydrogen bonds with the framework (H···F = 3.08 Å and 2.53 Å) while CO_2 has one close C···F contact (C···F distance = 2.99 Å). Lower enthalpies of adsorption were calculated for both gases (Figure S24). Importantly, we found that when SO_4^{2-} moieties were afforded freedom to rotate, alternating pairs of SO_4^{2-} pillars can synergistically orient an oxygen atom directly into a channel to optimally bind a C_2H_2 molecule, leaving alternating channels without SO_4^{2-} oxygen atoms pointing directly into them. That sulfate anions can rotate is experimentally supported by the crystal structure of **SOFOUR-1-Zn**, which exhibited disorder of the
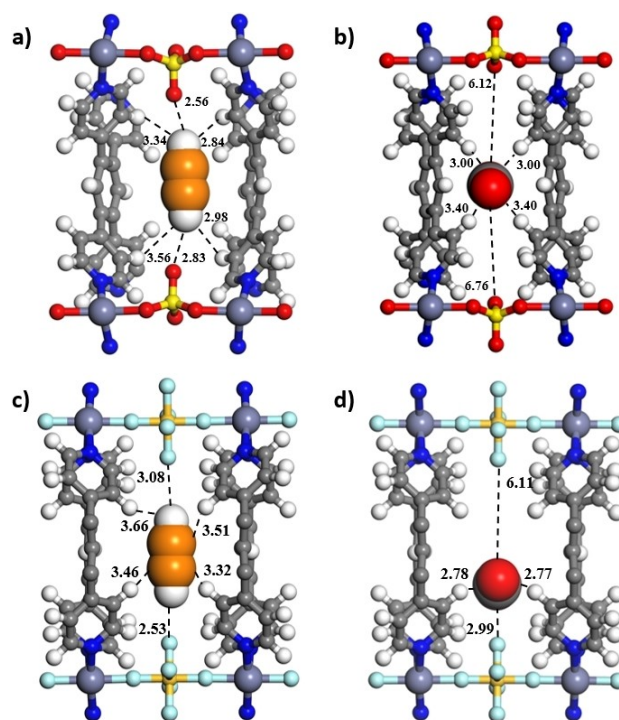

Figure 5. The binding sites of a) C_2H_2 and b) CO_2 in **SOFOUR-1-Zn** and c) C_2H_2 and d) CO_2 in **SIFSIX-22-Zn** obtained by DFT calculations. (Colour codes: N, blue; Si, gold; S, yellow; F, turquoise; Zn, lavender; O, red; H, white; C, grey and C (C_2H_2), orange. The distances are in Angstrom (Å). C_2H_2 and CO_2 molecules are shown in space-filling mode.

sulfate pillars (see Supporting Information for full details). Adsorption of C_2H_2 by the alternating pores with unfavourable electrostatics was calculated to be less exothermic. Such a binding mechanism would explain lower Q_{st} and reduced C_2H_2 uptake at higher loadings for **SOFOUR-1-Zn** vs. **SIFSIX-22-Zn** as the octahedral SiF_6^{2-} pillars preclude an alternating binding site arrangement (Figure S27).

Temperature swing cycling experiments revealed retention of breakthrough performance over three consecutive adsorption–desorption cycles (Figure S17), as well as good retention of the initial rates of sorption from gravimetric experiments. However, whereas both **SOFOUR-1-Zn** and **SIFSIX-22-Zn** were found to be stable to multiple regeneration cycles and storage under ambient conditions for at least 4 months (Figure S21), water vapor sorption isotherms conducted on both HUMs revealed that **SIFSIX-22-Zn** displayed a dramatic negative deviation in uptake at 80% R.H., corresponding with a phase transformation reminiscent of other well-studied HUMs (Fig S18).[31] In contrast, **SOFOUR-1-Zn** exhibited reversible Type I water sorption, with no discernible phase change occurring, although very minor peak broadening was observed by PXRD.

The stabilizing effect of the **SOFOUR** pillar is corroborated by PXRD studies on samples exposed to 75% R.H. and 313 K in line with previously reported accelerated moisture stability tests.[10c] We observed that **SIFSIX-22-Zn** underwent a phase change within 12 hours of exposure, whereas the onset of the phase change for **SOFOUR-1-Zn** occurred after 96 hours (Figure S19, S20). Therefore, the pillaring strategy outlined here resulted in improved stability and performance. In terms of the cost of manufacture, **tepb** can be prepared through a simple one-step synthesis (SI) although it is not widely commercially available. Mechanochemical synthesis of **SOFOUR-1-Zn** was attempted, but the material thus obtained exhibited limited porosity (Figure S22).

Conclusion

To conclude, we report the gram-scale room temperature synthesis of the prototypal sulfate-pillared HUM, **SOFOUR-1-Zn**. The use of sulfate pillars makes **SOFOUR-1-Zn** greener, cheaper, more stable, and more effective in the separation of C_2H_2 from CO_2 than previously reported materials and its **SIFSIX** analogue, **SIFSIX-22-Zn. SOFOUR-1-Zn** was found to exhibit benchmark performance in for trace separation of C_2H_2 from CO_2 and is the first sorbent that yields fuel grade C_2H_2 (>98% purity) from a 1:99 C_2H_2/CO_2 stream on desorption. DFT calculations provided insight into C_2H_2 binding in **SOFOUR-1-Zn**, revealing that it is enabled by $SO_4^{2-}\cdots C_2H_2$ H-bonding. This work reiterates that ultramicroporous physisorbents are highly effective for trace gas separations and demonstrates that they can be prepared using cheap and ubiquitous building blocks. Further research will focus on constructing SO_4^{2-}-pillared HUMs with commercially available linkers and improving their stability to humid conditions.

Conflict of Interest

The authors declare no conflict of interest.

Data Availability Statement

The data that support the findings of this study are available in the supplementary material of this article.

[1] a) S. Sircar, *Ind. Eng. Chem. Res.* **2006**, *45*, 5435–5448; b) J.-R. Li, R. J. Kuppler, H.-C. Zhou, *Chem. Soc. Rev.* **2009**, *38*, 1477–1504; c) S. Mukherjee, D. Sensharma, K.-J. Chen, M. J. Zaworotko, *Chem. Commun.* **2020**, *56*, 10419–10441; d) M. Y. Gao, B. Q. Song, D. Sensharma, M. J. Zaworotko, *SmartMat* **2021**, *2*, 38–55; e) Y. Wang, S. B. Peh, D. Zhao, *Small* **2019**, *15*, 1900058.

[2] S. Mukherjee, M. J. Zaworotko, *Trends Chem.* **2020**, *2*, 506–518.

[3] D. J. O'Hearn, A. Bajpai, M. J. Zaworotko, *Small* **2021**, *17*, 2006351.

[4] S. Subramanian, M. J. Zaworotko, *Angew. Chem. Int. Ed. Engl.* **1995**, *34*, 2127–2129; *Angew. Chem.* **1995**, *107*, 2295–2297.

[5] a) P. Nugent, Y. Belmabkhout, S. D. Burd, A. J. Cairns, R. Luebke, K. Forrest, T. Pham, S. Ma, B. Space, L. Wojtas, M. Eddaoudi, M. J. Zaworotko, *Nature* **2013**, *495*, 80–84; b) A. Bajpai, M. Lusi, M. J. Zaworotko, *Chem. Commun.* **2017**, *53*, 3978–3981; c) C. Gu, J. Liu, D. S. Sholl, *J. Phys. Chem. C* **2021**, *125*, 20076–20086; d) P. Nugent, V. Rhodus, T. Pham, B. Tudor, K. Forrest, L. Wojtas, B. Space, M. Zaworotko, *Chem. Commun.* **2013**, *49*, 1606–1608; e) P. A. Maggard, A. L. Kopf, C. L. Stern, K. R. Poeppelmeier, K. M. Ok, P. S. Halasyamani, *Inorg. Chem.* **2002**, *41*, 4852–4858; f) A. L. Kopf, P. A. Maggard, C. L. Stern, K. R. Poeppelmeier, *Acta Crystallogr. Sect. C* **2005**, *61*, m165–m168; g) A. Cadiau, Y. Belmabkhout, K. Adil, P. M. Bhatt, R. S. Pillai, A. Shkurenko, C. Martineau-Corcos, G. Maurin, M. Eddaoudi, *Science* **2017**, *356*, 731–735.

[6] a) M. H. Mohamed, S. K. Elsaidi, L. Wojtas, T. Pham, K. A. Forrest, B. Tudor, B. Space, M. J. Zaworotko, *J. Am. Chem. Soc.* **2012**, *134*, 19556–19559; b) M. H. Mohamed, S. K. Elsaidi, T. Pham, K. A. Forrest, B. Tudor, L. Wojtas, B. Space, M. J. Zaworotko, *Chem. Commun.* **2013**, *49*, 9809–9811.

[7] M. Lusi, P. B. Fechine, K.-J. Chen, J. J. Perry, M. J. Zaworotko, *Chem. Commun.* **2016**, *52*, 4160–4162.

[8] a) Q. Lin, C. Mao, A. Kong, X. Bu, X. Zhao, P. Feng, *J. Mater. Chem. A* **2017**, *5*, 21189–21195; b) L. He, J. K. Nath, Q. Lin, *Chem. Commun.* **2019**, *55*, 412–415; c) S. K. Elsaidi, M. H.

Mohamed, T. Pham, T. Hussein, L. Wojtas, M. J. Zaworotko, B. Space, *Cryst. Growth Des.* **2016**, *16*, 1071–1080.

[9] Q.-L. Qian, X.-W. Gu, J. Pei, H.-M. Wen, H. Wu, W. Zhou, B. Li, G. Qian, *J. Mater. Chem. A* **2021**, *9*, 9248–9255.

[10] a) S. Mukherjee, N. Sikdar, D. O'Nolan, D. M. Franz, V. Gascón, A. Kumar, N. Kumar, H. S. Scott, D. G. Madden, P. E. Kruger, B. Space, M. J. Zaworotko, *Sci. Adv.* **2019**, *5*, eaax9171; b) P. M. Bhatt, Y. Belmabkhout, A. Cadiau, K. Adil, O. Shekhah, A. Shkurenko, L. J. Barbour, M. Eddaoudi, *J. Am. Chem. Soc.* **2016**, *138*, 9301–9307; c) A. Kumar, C. Hua, D. G. Madden, D. O'Nolan, K.-J. Chen, L.-A. J. Keane, J. J. Perry, M. J. Zaworotko, *Chem. Commun.* **2017**, *53*, 5946–5949.

[11] D. G. Madden, D. O'Nolan, K.-J. Chen, C. Hua, A. Kumar, T. Pham, K. A. Forrest, B. Space, J. J. Perry, M. Khraisheh, M. J. Zaworotko, *Chem. Commun.* **2019**, *55*, 3219–3222.

[12] B. Li, X. Cui, D. O'Nolan, H. M. Wen, M. Jiang, R. Krishna, H. Wu, R. B. Lin, Y. S. Chen, D. Yuan, H. Xing, W. Zhou, Q. Ren, G. Qian, M. J. Zaworotko, B. Chen, *Adv. Mater.* **2017**, *29*, 1704210.

[13] a) H. S. Scott, M. Shivanna, A. Bajpai, D. G. Madden, K.-J. Chen, T. Pham, K. A. Forrest, A. Hogan, B. Space, J. J. Perry IV, M. J. Zaworotko, *ACS Appl. Mater. Interfaces* **2017**, *9*, 33395–33400; b) K.-J. Chen, H. S. Scott, D. G. Madden, T. Pham, A. Kumar, A. Bajpai, M. Lusi, K. A. Forrest, B. Space, J. J. Perry IV, M. J. Zaworotko, *Chem* **2016**, *1*, 753–765; c) R.-B. Lin, L. Li, H. Wu, H. Arman, B. Li, R.-G. Lin, W. Zhou, B. Chen, *J. Am. Chem. Soc.* **2017**, *139*, 8022–8028; d) N. Kumar, S. Mukherjee, N. C. Harvey-Reid, A. A. Bezrukov, K. Tan, V. Martins, M. Vandichel, T. Pham, L. M. van Wyk, K. Oyekan, A. Kumar, K. A. Forrest, K. M. Patil, L. J. Barbour, B. Space, Y. Huang, P. E. Kruger, M. J. Zaworotko, *Chem* **2021**, *7*, 3085–3098; e) Y. Zhang, J. Hu, R. Krishna, L. Wang, L. Yang, X. Cui, S. Duttwyler, H. Xing, *Angew. Chem. Int. Ed.* **2020**, *59*, 17664–17669; *Angew. Chem.* **2020**, *132*, 17817–17822.

[14] M. H. Mohamed, S. K. Elsaidi, T. Pham, K. A. Forrest, H. T. Schaef, A. Hogan, L. Wojtas, W. Xu, B. Space, M. J. Zaworotko, *Angew. Chem. Int. Ed.* **2016**, *55*, 8285–8289; *Angew. Chem.* **2016**, *128*, 8425–8429.

[15] a) C. Healy, N. C. Harvey-Reid, B. I. Howard, P. E. Kruger, *Dalton Trans.* **2020**, *49*, 17433–17439; b) C. Healy, K. M. Patil, B. H. Wilson, L. Hermanspahn, N. C. Harvey-Reid, B. I. Howard, C. Kleinjan, J. Kolien, F. Payet, S. G. Telfer, P. E. Kruger, T. D. Bennett, *Coord. Chem. Rev.* **2020**, *419*, 213388.

[16] L. Wang, W. Sun, Y. Zhang, N. Xu, R. Krishna, J. Hu, Y. Jiang, Y. He, H. Xing, *Angew. Chem. Int. Ed.* **2021**, *60*, 22865–22870; *Angew. Chem.* **2021**, *133*, 23047–23052.

[17] a) E. Davy, *The Transactions of the Royal Irish Academy* **1839**, 80–88; b) P. Pässler, W. Hefner, K. Buckl, H. Meinass, A. Meiswinkel, H. J. Wernicke, G. Ebersberg, R. Müller, J. Bässler, H. Behringer, *Ullmann's Encyclopedia of Industrial Chemistry*, Wiley-VCH, Weinheim, **2000**; c) H. Schobert, *Chem. Rev.* **2014**, *114*, 1743–1760.

[18] Q. Zhang, J. Wang, T. Wang, *Ind. Eng. Chem. Res.* **2016**, *55*, 8383–8394.

[19] W. M. Haynes, *CRC Handbook of Chemistry and Physics*, CRC, Boca Raton, **2014**.

[20] a) X.-P. Fu, Y.-L. Wang, Q.-Y. Liu, *Dalton Trans.* **2020**, *49*, 16598–16607; b) W. Fan, S. Yuan, W. Wang, L. Feng, X. Liu, X. Zhang, X. Wang, Z. Kang, F. Dai, D. Yuan, D. Sun, H.-C. Zhou, *J. Am. Chem. Soc.* **2020**, *142*, 8728–8737.

[21] D. L. Hilden, R. F. Stebar, *Int. J. Energy Res.* **1979**, *3*, 59–71.

[22] a) O. T. Qazvini, R. Babarao, S. G. Telfer, *Chem. Mater.* **2019**, *31*, 4919–4926; b) S. Mukherjee, Y. He, D. Franz, S. Q. Wang, W. R. Xian, A. A. Bezrukov, B. Space, Z. Xu, J. He, M. J. Zaworotko, *Chem. Eur. J.* **2020**, *26*, 4923–4929.

[23] a) D. Ma, Z. Li, J. Zhu, Y. Zhou, L. Chen, X. Mai, M. Liufu, Y. Wu, Y. Li, *J. Mater. Chem. A* **2020**, *8*, 11933–11937; b) Y. Xie, H. Cui, H. Wu, R. B. Lin, W. Zhou, B. Chen, *Angew. Chem. Int. Ed.* **2021**, *60*, 9604–9609; *Angew. Chem.* **2021**, *133*, 9690–9695; c) L. Li, J. Wang, Z. Zhang, Q. Yang, Y. Yang, B. Su, Z. Bao, Q. Ren, *ACS Appl. Mater. Interfaces* **2018**, *11*, 2543–2550.

[24] Deposition Number(s) 2105435 (for **SOFOUR-1-Zn**) and 2069812 (for **SIFSIX-22-Zn**) contain the supplementary crystallographic data for this paper. These data are provided free of charge by the joint Cambridge Crystallographic Data Centre and Fachinformationszentrum Karlsruhe Access Structures service www.ccdc.cam.ac.uk/structures.

[25] C. R. Groom, I. J. Bruno, M. P. Lightfoot, S. C. Ward, *Acta Crystallogr. Sect. B* **2016**, *72*, 171–179.

[26] a) P. Zhou, Z. Anorg. Allg. Chem. **2017**, *643*, 653–656; b) L.-W. Lee, T.-T. Luo, C.-M. Wang, G.-H. Lee, S.-M. Peng, Y.-H. Liu, S.-L. Lee, K.-L. Lu, *J. Solid State Chem.* **2016**, *239*, 1–7; c) D. Bradshaw, J. E. Warren, M. J. Rosseinsky, *Science* **2007**, *315*, 977–980; d) A. Dey, A. Garai, V. Gude, K. Biradha, *Cryst. Growth Des.* **2018**, *18*, 6070–6077.

[27] S. Hu, Z.-M. Zhang, Z.-S. Meng, Z.-J. Lin, M.-L. Tong, *CrystEngComm* **2010**, *12*, 4378–4385.

[28] Y. L. Peng, T. Pham, P. Li, T. Wang, Y. Chen, K. J. Chen, K. A. Forrest, B. Space, P. Cheng, M. J. Zaworotko, Z. Zhang, *Angew. Chem. Int. Ed.* **2018**, *57*, 10971–10975; *Angew. Chem.* **2018**, *130*, 11137–11141.

[29] a) N. Kumar, S. Mukherjee, A. A. Bezrukov, M. Vandichel, M. Shivanna, D. Sensharma, A. Bajpai, V. Gascón, K.-I. Otake, S. Kitagawa, M. J. Zaworotko, *Smart Mater. Struct.* **2020**, *1*, e1008; b) L. Yang, L. Yan, Y. Wang, Z. Liu, J. He, Q. Fu, D. Liu, X. Gu, P. Dai, L. Li, *Angew. Chem. Int. Ed.* **2021**, *60*, 4570–4574; *Angew. Chem.* **2021**, *133*, 4620–4624.

[30] a) S. Sharma, S. Mukherjee, A. V. Desai, M. Vandichel, G. K. Dam, A. Jadhav, G. Kociok-Köhn, M. J. Zaworotko, S. K. Ghosh, *Chem. Mater.* **2021**, *33*, 5800–5808; b) J. Pei, K. Shao, J. X. Wang, H. M. Wen, Y. Yang, Y. Cui, R. Krishna, B. Li, G. Qian, *Adv. Mater.* **2020**, *32*, 1908275; c) P. Li, Y. He, Y. Zhao, L. Weng, H. Wang, R. Krishna, H. Wu, W. Zhou, M. O'Keeffe, Y. Han, B. Chen, *Angew. Chem. Int. Ed.* **2015**, *54*, 574–577; *Angew. Chem.* **2015**, *127*, 584–587.

[31] D. O'Nolan, A. Kumar, M. J. Zaworotko, *J. Am. Chem. Soc.* **2017**, *139*, 8508–8513.